The Astrophysical Journal, 609:335–339, 2004 July 1

PULSAR RADIO EMISSION ALTITUDE FROM CURVATURE RADIATION

R. T. Gangadhara
Indian Institute of Astrophysics, Koramangala, II Block, Bangalore 560034, India; ganga@iiap.res.in
Received 2003 October 17; accepted 2004 March 11

ABSTRACT

We assume that relativistic sources moving along dipolar magnetic field lines emit curvature radiation. The beamed emission occurs in the direction of tangents to the field lines, and to receive it, the sight line must align with the tangent within the beaming angle $1/\gamma$, where γ is the particle Lorentz factor. By solving the viewing geometry in an inclined and rotating dipolar magnetic field, we show that at any given pulse phase, the observer tends to receive radiation only from the specific heights allowed by the geometry. We find that outer conal components are emitted at higher altitudes compared to inner components, including the core. At any pulse phase, low-frequency emission comes from higher altitudes than high-frequency emission. We have modeled the emission heights of pulse components of PSR B0329+54 and estimated field line curvature radii and particle Lorentz factors in the emission regions.

Subject headings: pulsars: general — pulsars: individual (PSR B0329+54) — radio continuum: stars — stars: magnetic fields

1. INTRODUCTION

Pulsar radio emission is generally thought to be coherent radiation from relativistic plasma streaming along open magnetic field lines. It has been widely attempted to interpret the emission beam geometry in terms of emission in a purely dipolar magnetic field (e.g., Radhakrishnan & Cooke 1969; Goldreich & Julian 1969; Sturrock 1971; Ruderman & Sutherland 1975; Michel 1982; Blaskiewicz et al. 1991).

Radhakrishnan & Cooke (1969) have proposed the rotating vector model (RVM) to explain the polarization-angle (PA) traverse (S-curve) of pulsar profiles. It has been fitted to average PA curves and found to be quite successful (e.g., Lyne & Manchester 1988). The three chief assumptions (Hibschman & Arons 2001) of the RVM model are (1) the relativistic plasma flow is collimated by strong dipolar magnetic field lines, (2) the observed radiation is beamed in the direction of tangents to the field lines, and (3) the polarization angle is at a fixed angle to the curvature of field lines, as is the case for vacuum curvature radiation. Based on assumptions (1) and (2), we have attempted to locate the radio emission region in the pulsar magnetosphere from which a distant observer receives the radiation.

Statistical analysis of the distribution of pulse components within the pulse window indicates that the emission beam is conal (e.g., Mitra & Deshpande 1999; Kijak & Gil 2002). Rankin (1993) has indicated that inner pulse components are emitted at lower altitudes than the outer ones. Gangadhara & Gupta (2001; hereafter GG01) have estimated the emission height of different radio pulse components of PSR B0329+54 based on the aberration-retardation phase shift. They have also found that the inner components of pulse profiles originate from lower altitudes than the outer components. In their following paper, Gupta & Gangadhara (2003) have then estimated the emission heights of six more pulsars using the same technique. Recently, the emission heights of all of those pulsars have been re-estimated by Dyks et al. (2004; hereafter DRH04) by revising the aberration phase-shift relation given in GG01. There are also other claims for core and cone emission altitudes being different (e.g., Mitra & Rankin 2002) and roughly the same (e.g., Gil 1991).

In this paper, we solve the viewing geometry for receiving the radio waves by a distant observer in § 2. By assuming the particle Lorentz factors, we show in § 2.2 that curvature radiation predicts the emission heights that are comparable to the radio emission heights in PSR B0329+54. In § 3, by utilizing the properties of curvature radiation and the emission altitudes estimated from aberration-retardation phase shifts (DRH04), we estimate the field line curvature radii and particle Lorentz factors in the emission region.

2. EMISSION-BEAM GEOMETRY

Consider a magnetic dipole situated at the origin with magnetic dipole moment $\hat{\boldsymbol{m}}$ aligned with the rotation axis ($\hat{\boldsymbol{\Omega}}$). In polar coordinates, the equation for a dipolar field line (Alfvén & Falthämmar 1963) is $r = r_e \sin^2\theta$, where θ is the magnetic colatitude and r the distance from the origin. The parameter r_e is the *field line constant*, which is the distance from the origin to the point of the field line intersection with the equatorial plane ($\theta = \pi/2$). In the case of an aligned dipole, $r_e = r_{\rm LC}$ for the last open field line, where $r_{\rm LC} = Pc/2\pi$ is the light cylinder radius, c the speed of light, and P the pulsar period. In a Cartesian coordinate system with the z-axis parallel to $\hat{\boldsymbol{\Omega}}$, the position vector of an arbitrary point Q on a field line is given by

$$\boldsymbol{r}_c = r_e(\sin^3\theta\cos\phi,\ \sin^3\theta\sin\phi,\ \sin^2\theta\cos\theta), \qquad (1)$$

where ϕ is the magnetic azimuth.

Now consider the situation where the dipole $\hat{\boldsymbol{m}}$ is *inclined* through an angle α with respect to $\hat{\boldsymbol{\Omega}}$ and *rotated* by phase ϕ' around the z-axis, as shown in Figure 1. The position vector of the point Q on a magnetic field line that is tilted and rotated is given by

$$\boldsymbol{r}_{ct} = \Lambda \cdot \boldsymbol{r}_c, \qquad (2)$$

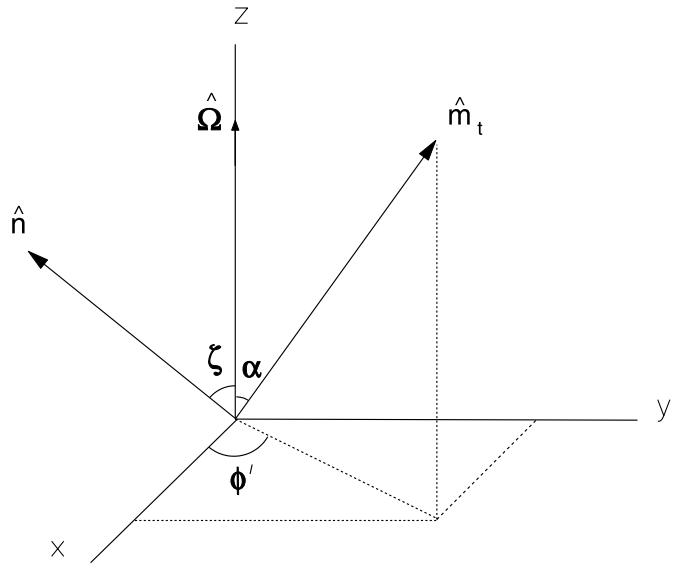

FIG. 1.—Coordinate system that describes the inclined and rotating magnetic dipole. The rotation phase ϕ' is measured from the fiducial plane (x-z) in the counterclockwise direction around $\hat{\boldsymbol{\Omega}}$. The magnetic colatitude θ is measured from $\hat{\boldsymbol{m}}_t$, and the magnetic azimuth ϕ is measured counterclockwise around $\hat{\boldsymbol{m}}_t$ from the meridional plane defined by $\hat{\boldsymbol{\Omega}}$ and $\hat{\boldsymbol{m}}_t$.

where the transformation matrix $\Lambda = R \cdot I$. The matrices for tilt (inclination) I and rotation R are given by

$$I = \begin{pmatrix} \cos\alpha & 0 & \sin\alpha \\ 0 & 1 & 0 \\ -\sin\alpha & 0 & \cos\alpha \end{pmatrix},$$

$$R = \begin{pmatrix} \cos\phi' & -\sin\phi' & 0 \\ \sin\phi' & \cos\phi' & 0 \\ 0 & 0 & 1 \end{pmatrix}. \tag{3}$$

The matrix I produces clockwise rotation of the dipole around the y-axis, and R produces counterclockwise rotation around the z-axis.

At Q, we find the *tangent* to the field line by evaluating $\boldsymbol{b}_t = \partial \boldsymbol{r}_{\zeta t}/\partial\theta$ and the *curvature* by evaluating $\boldsymbol{k}_t = d\hat{\boldsymbol{b}}_t/ds$, where $\hat{\boldsymbol{b}}_t = \boldsymbol{b}_t/|\boldsymbol{b}_t|$ is a unit tangent vector, ds is the arc length of the field line, and

$$|\boldsymbol{b}_t| = r_e\sqrt{5 + 3\cos(2\theta)}\sin\theta/\sqrt{2}.$$

Therefore, the field line curvature radius is given by

$$\rho = \frac{1}{|\boldsymbol{k}_t|} = \frac{r_e \sin\theta[5 + 3\cos(2\theta)]^{3/2}}{3\sqrt{2}[3 + \cos(2\theta)]}. \tag{4}$$

Since $\hat{\boldsymbol{m}}$ is chosen to be parallel to $\hat{\boldsymbol{z}}$, the transformed magnetic dipole moment is given by

$$\hat{\boldsymbol{m}}_t = \Lambda \cdot \hat{\boldsymbol{z}} = (\sin\alpha\cos\phi',\ \sin\alpha\sin\phi',\ \cos\alpha). \tag{5}$$

Hence, the magnetic field of a dipole (Jackson 1975) that is inclined and rotated is given by

$$\boldsymbol{B}_t = B_0\left(\frac{r_{\rm NS}}{r}\right)^3[3(\hat{\boldsymbol{r}}\cdot\hat{\boldsymbol{m}}_t)\hat{\boldsymbol{r}} - \hat{\boldsymbol{m}}_t], \tag{6}$$

where B_0 is the surface magnetic field and $r_{\rm NS} \sim 10$ km is the neutron star radius. It can be easily shown that $\boldsymbol{B}_t$ satisfies $\nabla \cdot \boldsymbol{B}_t = 0$.

The dominant magnetic field in the emission region is often shown to be consistent with being dipolar and is used to study the shape of pulsar radio beams (e.g., Narayan & Vivekanand 1983; Lyne & Manchester 1988; Kramer et al. 1997). In a static dipolar magnetic field approximation, the basic features of the pulsar magnetosphere can be understood. On the timescales of the order of the pulse-phase bin, which is very small compared to the pulsar period, the rotating dipole can be treated approximately as a static dipole.

2.1. *Magnetic Colatitude and Azimuth of Emission Spot*

Consider the sight line $\hat{\boldsymbol{n}} = (\sin\zeta, 0, \cos\zeta)$ that lies in the x-z plane and makes an angle ζ with respect to $\hat{\boldsymbol{\Omega}}$, where $\zeta = \alpha + \beta$ and β is the angle of closest approach of the sight line with respect to the magnetic axis. The half-opening angle Γ of the emission beam is given by

$$\cos\Gamma = \hat{\boldsymbol{n}}\cdot\hat{\boldsymbol{m}}_t = \cos\alpha\cos\zeta + \sin\alpha\sin\zeta\cos\phi'. \tag{7}$$

If τ is the angle between $\hat{\boldsymbol{b}}_t$ and $\hat{\boldsymbol{m}}_t$, then we have

$$\cos\tau = \hat{\boldsymbol{b}}_t\cdot\hat{\boldsymbol{m}}_t = \frac{1 + 3\cos(2\theta)}{\sqrt{10 + 6\cos(2\theta)}}. \tag{8}$$

In a relativistic flow, radiation is beamed in the direction of the field line tangent. Thus, at any instant, observable radiation comes from a spot in the magnetosphere where the tangent vector $\hat{\boldsymbol{b}}_t$ points in the direction of $\hat{\boldsymbol{n}}$. That is, $\Gamma \approx \tau$ at the emission spot. Therefore, using equations (7) and (8), we can find the relation for *magnetic colatitude* θ as a function of Γ:

$$\cos(2\theta) = \frac{1}{3}(\cos\Gamma\sqrt{8 + \cos^2\Gamma} - \sin^2\Gamma), \quad -\pi \le \Gamma \le \pi. \tag{9}$$

This equation is similar to the one given in GG01 (see eq. [4]) for θ. However, equation (9) is superior compared to GG01's equation, as it represents a single physical solution when Γ changes sign. For $\Gamma \ll 1$, equation (9) reduces to the well-known approximate form $\theta \approx (2/3)\Gamma$.

Next, let κ be the angle between $\hat{\boldsymbol{n}}$ and $\hat{\boldsymbol{b}}_t$; then we have

$$\begin{aligned}\cos\kappa &= \hat{\boldsymbol{n}}\cdot\hat{\boldsymbol{b}}_t \\ &= \cos^2\Gamma + (\cos\alpha\sin\zeta\cos\phi' - \sin\alpha\cos\zeta)\sin\Gamma\cos\phi \\ &\quad - \sin\zeta\sin\phi'\sin\Gamma\sin\phi. \end{aligned}\tag{10}$$

Again, to receive the radiation, κ must be ~ 0. Therefore, we find the *magnetic azimuth* ϕ of the emission spot by solving $\hat{\boldsymbol{n}}\cdot\hat{\boldsymbol{b}}_t = 1$ and $\hat{\boldsymbol{n}} \times \hat{\boldsymbol{b}}_t = 0$:

$$\begin{aligned}\sin\phi &= -\sin\zeta\sin\phi'\csc\Gamma, \\ \cos\phi &= (\cos\alpha\sin\zeta\cos\phi' - \cos\zeta\sin\alpha)\csc\Gamma.\end{aligned}$$

Therefore, we have

$$\phi = \arctan\left(\frac{\sin\zeta\sin\phi'}{\cos\zeta\sin\alpha - \cos\alpha\sin\zeta\cos\phi'}\right). \tag{11}$$

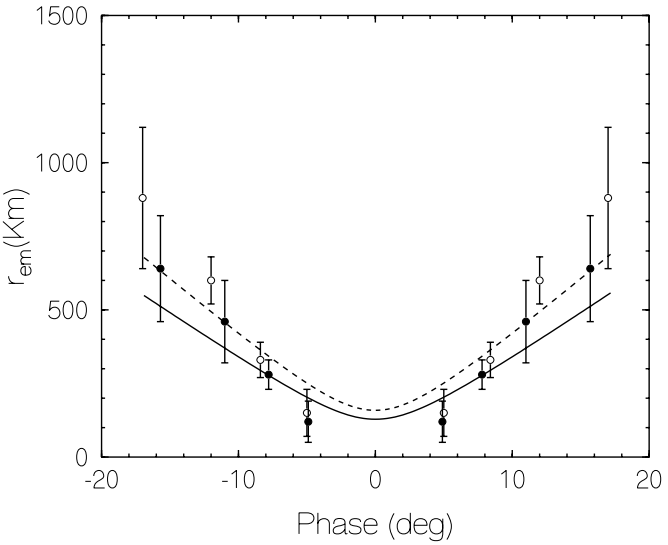

FIG. 2.—Radio wave emission heights in PSR B0329+54 with respect to rotation phase ϕ'. Solid and dashed curves are for the emissions at 606 and 325 MHz, respectively. The emission heights estimated from aberration-retardation phase shift (DRH04) are superposed for comparison: the points marked with open and filled circles are for the components at 325 and 606 MHz, respectively.

Note that ϕ is measured with respect to the meridional plane defined by $\hat{\boldsymbol{\Omega}}$ and $\hat{\boldsymbol{m}}_t$.

2.2. *Radio Emission Height*

Pulsar radio emission is generally believed to be coherent curvature radiation emitted by secondary-pair plasma streaming along the dipolar magnetic field lines. The characteristic frequency of curvature radiation, at which the emission peaks, is given by

$$\nu = \frac{3c}{4\pi}\frac{\gamma^3}{\rho} \tag{12}$$

(Ruderman & Sutherland 1975), where γ and ρ are the Lorentz factor and the radius of curvature of the trajectory of a relativistic particle, respectively. Since particles closely follow the curved dipolar field lines, the curvature of a particle's trajectory can be approximated with the curvature of field lines.

For the given ν and γ, equation (12) predicts the value of ρ required. Then, using equation (4), we can find the field line constant r_e with the help of the value of $\theta_{\rm em}$ obtained from equation (9). The azimuth $\phi_{\rm em}$ of the emission spot can be determined by using equation (11). Hence, by having defined $(r_e, \theta_{\rm em}, \phi_{\rm em})$, we can estimate the emission height $r_{\rm em}$ of radio waves of frequency ν with respect to pulse phase ϕ' by using equation (2).

Based on the aberration-retardation phase shift of pulse components in observed profiles, GG01 have estimated the emission heights of pulse components in PSR B0329+54 at frequencies of 325 and 606 MHz. Recently, DRH04 have revised the aberration phase-shift relation given in GG01 and re-estimated the emission heights. In Figure 2, we have plotted the revised emission heights (*circles with error bars*).

To model the emission heights in PSR B0329+54, we adopt the value of $(\alpha,\ \beta) = (30^\circ,\ 2^\circ.1)$ given by Rankin (1993). We find that the curvature emission predicts the emission heights (Fig. 2, *solid and dashed curves*) that are comparable to the observed ones (DRH04) if the secondary-particle Lorentz factor $\gamma \approx 340$ and 390 for the emissions at 325 and 606 MHz, respectively. Figure 2 shows that at any given frequency, the emission near the pulse center (core) comes from lower heights compared to outer conal components, in agreement with the results derived from observations (Fig. 2, *circles*). At any pulse phase, low-frequency emission comes from a higher altitude than high-frequency emission, in agreement with the well-known radius-to-frequency mapping (RFM; e.g., Cordes 1978; Phillips 1992). We find that RFM is not uniform across the pulse window; i.e., it is more pronounced in the case of outer cones (say, cones 3 and 4) than in the inner cones (say, cones 1 and 2). Mitra & Rankin (2002) have also made a similar proposition from the study of 10 selected pulsars. The emission height difference $\delta r_{\rm em}$ between the two frequencies increases progressively with respect to pulse phase, and the circles in Figure 2 indicate that $\delta r_{\rm em} \approx 14 + 0.046(\phi')^2 + 0.003(\phi')^4$ km, where the pulse phase ϕ' is in degrees.

2.3. *The Polar Cap*

The polar cap boundary is defined by the last open field lines for which $\boldsymbol{k}_t \cdot \hat{\boldsymbol{z}} = 0$ at the light cylinder. Therefore, the magnetic colatitude $\theta_{\rm lof} = \theta$ at which $\boldsymbol{k}_t \cdot \hat{\boldsymbol{z}}$ vanishes is given by

$$\cos(2\theta_{\rm lof}) = \frac{-3a_1^2 - a_2\sqrt{8a_1^2 + a_2^2}}{9a_1^2 + a_2^2}, \quad -\frac{\pi}{2} < \phi \le \frac{\pi}{2}, \tag{13}$$

where $a_1 = \sin\alpha\cos\phi$ and $a_2 = 3\cos\alpha$. Next, for the range of $\pi/2 < \phi \le 3\pi/2$, the colatitude is given by $\pi - \theta_{\rm lof}$. The angle η between $\hat{\boldsymbol{r}}_{ct}$ and $\hat{\boldsymbol{z}}$ is given by

$$\cos\eta = \hat{\boldsymbol{z}} \cdot \hat{\boldsymbol{r}}_{ct} = \cos\alpha\cos\theta - \sin\alpha\sin\theta\cos\phi. \tag{14}$$

If $\eta_{\rm lof} = \eta$ at the light cylinder for the last open field line, then we have $|\boldsymbol{r}_{ct}|\sin\eta_{\rm lof} = r_{\rm LC}$, and the last open field line constant

$$r_{e,\,\rm lof} = r_{\rm LC}\csc^2\theta_{\rm lof}\csc\eta_{\rm lof}. \tag{15}$$

Hence, the radial position of the foot of the last open field line from the magnetic axis is given by

$$s_p = r_{\rm NS}\theta_p, \tag{16}$$

where $\theta_p = \arcsin\left[(r_{\rm NS}/r_{e,\,\rm lof})^{1/2}\right]$ is the colatitude of the foot of the last open field line.

To plot the polar cap, consider the Cartesian coordinate system $(x_B,\ y_B,\ z_B)$ such that the axis z_B is parallel to $\hat{\boldsymbol{m}}_t$ and x_B lies in the meridional plane. The coordinates of the foot of the last open field line are given by

$$(x_B,\ y_B) = (s_p\cos\phi,\ s_p\sin\phi). \tag{17}$$

Using $\alpha = 30^\circ$, the polar cap of PSR B0329+54 is plotted in Figure 3. It is quasi-elliptical, with the dimension of 164 m in the x_B direction and 171 m in the direction of y_B, in agreement with the polar cap shapes proposed by Biggs (1990).

For a given pulse phase ϕ', by using equations (9) and (11), we can find $\theta_{\rm em}$ and $\phi_{\rm em}$ of the emission spot. The radial

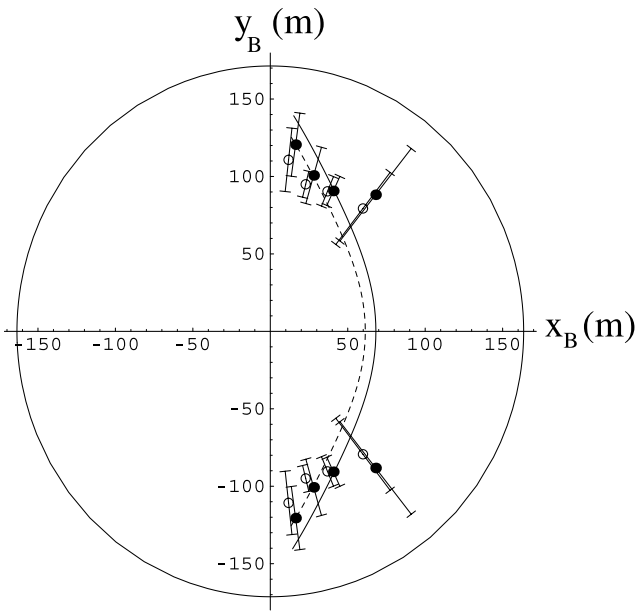

FIG. 3.—Polar cap of PSR B0329+54. Solid and dashed curves represent the locus of the feet of field lines associated with the emissions at 606 and 325 MHz, respectively. The values of $s_{\rm em}$ estimated from aberration-retardation phase shifts are superposed for comparison: the points marked with open and filled circles are for 325 and 606 MHz, respectively.

location of the foot of the field lines, from which a distant observer receives the radiation, is given by

$$s_{\rm em} = \sqrt{\frac{r_{\rm NS}^3}{r_{\rm em}}} \sin\theta_{\rm em}. \qquad (18)$$

Thus, by knowing $s_{\rm em}$ and $\phi_{\rm em}$, one can specify $(x_B,\ y_B)$ of the foot of the field lines that direct the radiation beam toward the observer. The values of $s_{\rm em}$ estimated from the conal aberration-retardation phase shift (*circles with error bars*) are plotted in Figure 3. The model (*dashed and solid*) curves represent the locus of the feet of those field lines that are accessible to a distant observer in 325 and 606 MHz observations, respectively. We find that the low-frequency emission is received from the field lines that lie closer to the magnetic axis than the high-frequency ones. The curve (*solid line*) indicates increasing conal ring spacing ($\delta s_{\rm em}$) between the successive rings from inner (cone 1) to outer (cone 4) on the polar cap: $\sim$14 m between the first and second rings, 16 m between the second and third, and 19 m between the third and fourth. The dashed curve for 325 MHz emission also indicates similar ring spacings, except they are less by $\sim$0.5 m. These results tend to support the model of concentric rings of sparks produced in the vacuum gap region just above the neutron surface (e.g., Ruderman & Sutherland 1975; Gil & Sendyk 2000).

3. DISCUSSION

In the previous section, to explain the emission height of the components in PSR B0329+54, we selected a Lorentz factor γ of about 340 and 390 for the emissions at 325 and 606 MHz, respectively. It means that ρ and γ assume constant values across the pulse window. However, it may not be reality, as the model heights significantly depart from the observed ones (*circles*) indicated in Figure 2. On the other hand, one can turn around the calculation by accepting the observed emission heights and asking for the required γ and ρ. In column (2) of Tables 1 and 2, we have given the phase location of conal components in the absence of an aberration-retardation phase shift (see eq. [11] of GG01), i.e., in a corotating frame. Next, columns (3) and (4) give the magnetic colatitude θ and the longitude ϕ of the emission spot, respectively, as estimated using equations (9) and (11). The small values of $\theta < 6^\circ$ implies that the conal emission mostly comes from the vicinity of the magnetic axis. By having known $r_{\rm em}$ and $\theta_{\rm em}$, we estimated the radius of curvature ρ using equation (4), the values of which are given in column (5). It shows that inner cones are emitted from the region of smaller curvature than are outer ones. Next, for a given frequency ν and known ρ, equation (12) allows us to estimate the γ of secondary particles, the values of which are given in column (6). It shows how particles with slightly higher γ move on the field lines associated with outer cones rather than inner cones.

The emission beam produced by relativistic particles is centered on their velocity, which is roughly parallel to the field line tangent $\hat{\boldsymbol{b}}_t$, and has a radial angular width of $1/\gamma$. Consequently, an observer tends to receive the radiation even when $\hat{\boldsymbol{n}}$ does not perfectly align with $\hat{\boldsymbol{b}}_t$, which can lead to a spread in the emission height, as well as in the pulse phase of the component peak location. Thus, we estimated the spread of the emission height of conal components by allowing Γ in equation (9) to vary by $1/\gamma$. However, we find that the spread is minimal and lies within the error bars. For example, at 325 MHz, we find it to be 9 km for the first cone and 15 km for the fourth cone. At 606 MHz, it is 6 km for the first cone and 10 km for the fourth. For the other cones, the spread lies in between these values. We also estimated the spread in the phase of the component peaks and found it to be less than $0^\circ.4$ for all the components. If we compare the emission heights (DRH04) along with these spreads, we find that the emission regions of conal components at the two frequencies are well separated, by 14 km in the case of the first and 214 km for the fourth. Furthermore, the pulse phase locations of conal components are different at the two frequencies, as indicated in column (2) in Tables 1 and 2. Thus, the observer tends to see

TABLE 1

PARAMETERS RELATED TO RADIO EMISSION FROM PSR B0329+54 AT 325 MHz

Cone Number (1)	ϕ' (deg) (2)	θ (deg) (3)	ϕ (deg) (4)	$\rho/r_{\rm LC}$ (5)	γ (6)	P/P_1[a] (7)
1.....	5.0 ± 0.26	2.22 ± 0.07	-53.0 ± 1.6	0.15 ± 0.00	286 ± 3	1.00 ± 0.08
2.....	8.4 ± 0.19	3.21 ± 0.06	-67.8 ± 0.6	0.23 ± 0.00	329 ± 2	0.76 ± 0.03
3.....	12.0 ± 0.27	4.35 ± 0.09	-76.5 ± 0.5	0.31 ± 0.01	363 ± 2	0.62 ± 0.03
4.....	17.0 ± 0.80	5.99 ± 0.26	-83.9 ± 1.0	0.33 ± 0.01	370 ± 5	0.60 ± 0.06

[a] $P_1 = 1.16 \times 10^{-16}$ ergs s^{-1}.

TABLE 2
PARAMETERS RELATED TO RADIO EMISSION FROM PSR B0329+54 AT 606 MHz

Cone Number (1)	ϕ' (deg) (2)	θ (deg) (3)	ϕ (deg) (4)	ρ/r_{LC} (5)	γ (6)	P/P_1[a] (7)
1.....	4.9 ± 0.25	2.19 ± 0.07	-52.4 ± 1.6	0.12 ± 0.00	328 ± 3	1.00 ± 0.07
2.....	7.8 ± 0.18	3.02 ± 0.06	-65.8 ± 0.6	0.21 ± 0.00	391 ± 2	0.70 ± 0.03
3.....	11.0 ± 0.45	4.02 ± 0.14	-74.5 ± 1.0	0.26 ± 0.01	419 ± 5	0.61 ± 0.05
4.....	15.7 ± 0.59	5.56 ± 0.19	-82.3 ± 0.8	0.26 ± 0.01	420 ± 5	0.61 ± 0.05

[a] $P_1 = 3.06 \times 10^{-16}$ ergs s^{-1}.

the components separated in phase as well. Note that the received radiation is at a maximum only when $\hat{\boldsymbol{n}}$ perfectly aligns with $\hat{\boldsymbol{b}}_t$. Hence, we can conclude that the observer tends to receive the radiation at the two frequencies from two distinct regions in the magnetosphere.

Using these values of γ and ρ, we estimated the power radiated by an electron or a positron from curvature emission (see eq. [25a] of Ruderman & Sutherland 1975), which is given in column (7) of the tables. It shows that the single particle emission is at a maximum in the region of the inner cone than in the outer cone regions. However, we know from the estimates made by Ruderman & Sutherland (1975) that the incoherent superposition of single particle radiation cannot explain the pulsar radio emission. The very high brightness temperature (10^{25}–10^{30} K) of pulsars leads to the conclusion that it must be coherent. The coherence due to the bunching of plasma particles in the magnetosphere was proposed much earlier (e.g., Pacini & Rees 1970; Sturrock 1971). The coherence due to bunching goes as the inverse of the wavelength of radio waves; therefore, the emission by bunches at low frequency tends to dominate the high-frequency emission.

Thus, we have developed a method for estimating the possible values of γ and ρ needed for the emission of radio waves at a given frequency. By matching the coherent curvature emission with the observed pulsar fluxes, one may be able to estimate the plasma density and the coherency (bunching) factor that exist in the radio emission region of pulsars. For $\nu \geq \nu_p$, strong coherent radiation occurs, where ν_p is the plasma frequency (Ruderman & Sutherland 1975).

While estimating the aberration-retardation phase shift of conal components, the core (reference) phase was set to zero (GG01; DRH04). However, it is possible that the core is also emitted at a finite height from the neutron star surface, as indicated by Figure 2. We fitted a fourth-degree polynomial to the emission heights (Fig. 2, *circles*) of eight conal components. At zero phase, the fit indicated an emission height of 26 ± 50 km for the 325 MHz points and 12 ± 45 km for the 606 MHz points. These heights can be treated as minimum values for the core emission height, as the component heights themselves have been estimated by setting the core phase to zero. Although it is important to consider the emission height of the core phase, we believe our results will not be changed significantly by the core height, as aberration and retardation are minimal at that height.

4. CONCLUSION

By assuming that the curvature emission by relativistic sources is beamed in the direction of a tangent to the dipolar magnetic field lines, we have resolved the pulsar radio emission geometry by solving the viewing geometry in an inclined and rotating dipolar magnetic field. Because of the geometric restrictions, a distant observer tends to receive outer conal components from higher altitudes than inner ones, including the core. Furthermore, we find that low-frequency emission comes from higher altitudes than high-frequency emission, in agreement with the radius-to-frequency mapping (RFM). We find that RFM is more pronounced in the outer conal components than in the inner ones. Using the emission heights obtained from aberration-retardation phase shifts, we have estimated the probable values of the Lorentz factors and field line curvature radii in the emission region.

I would like to thank Don Melrose and Simon Johnston for illuminating discussions and J. M. Rankin, J. A. Gil, Y. Gupta, V. Krishan, and C. Sivaram for comments. I thank the anonymous referee for useful comments.

REFERENCES

Alfvén, H., & Falthämmar, C.-G. 1963, Cosmical Electrodynamics (2nd ed.; Oxford: Clarendon Press)
Biggs, J. D. 1990, MNRAS, 245, 514
Blaskiewicz, M., Cordes, J. M., & Wasserman, I. 1991, ApJ, 370, 643
Cordes, J. M. 1978, ApJ, 222, 1006
Dyks, J., Rudak, B., & Harding, A. K. 2004, ApJ, 607, 939 (DRH04)
Gangadhara, R. T., & Gupta, Y. 2001, ApJ, 555, 31 (GG01)
Gil, J. A. 1991, A&A, 243, 219
Gil, J. A., & Sendyk, M. 2000, ApJ, 541, 351
Goldreich, P., & Julian, W. H. 1969, ApJ, 157, 869
Gupta, Y., & Gangadhara, R. T. 2003, ApJ, 584, 418
Hibschman, J. A., & Arons, J. 2001, ApJ, 546, 382
Jackson, J. D. 1975, Classical Electrodynamics (New York: Wiley)
Kijak, J., & Gil, J. 2002, A&A, 392, 189
Kramer, M., et al. 1997, A&A, 322, 846
Lyne, A. G., & Manchester, R. N. 1988, MNRAS, 234, 477
Michel, F. C. 1982, Rev. Mod. Phys., 54, 1
Mitra, D., & Deshpande, A. A. 1999, A&A, 346, 906
Mitra, D., & Rankin, J. M. 2002, ApJ, 577, 322
Narayan, R., & Vivekanand, M. 1983, A&A, 122, 45
Pacini, F., & Rees, M. J. 1970, Nature, 226, 622
Phillips, J. A. 1992, ApJ, 385, 282
Radhakrishnan, V., & Cooke, D. J. 1969, ApJ, 3, L225
Rankin, J. M. 1993, ApJ, 405, 285
Ruderman, M. A., & Sutherland, P. G. 1975, ApJ, 196, 51
Sturrock, P. A. 1971, ApJ, 164, 529